RSC Advances

PAPER

Cite this: *RSC Adv.*, 2015, **5**, 44960

Microcrystalline β-$RbNd(MoO_4)_2$: spin polarizing DFT+*U*

A. H. Reshak[ab]

Using density functional theory plus the Hubbard Hamiltonian (*U*), we have investigated the spin up (↑) and spin down (↓) electronic band structure, density of states, electronic charge density distribution and dispersion of the optical properties of microcrystalline β-$RbNd(MoO_4)_2$. We have applied *U* on the 4f orbital of Nd atoms and 4d orbital of Mo atoms. The calculated electronic band structure indicates that β-$RbNd(MoO_4)_2$ is a direct band gap semiconductor with a spin up (↑) energy gap which is lower than that of the spin down (↓). This is attributed to the different location of Nd-f in the spin up (↑) than the spin down (↓) case. The total valence charge density distribution in the (1 0 0) and (1 0 1) crystallographic planes for spin up (↑) and spin down (↓) were analyzed. The calculated bond distances show good agreement with the measured ones. The optical properties were investigated to seek deep insight into the electronic structure. It was found that the β-$RbNd(MoO_4)_2$ crystal exhibits negative uniaxial anisotropy and shows a lossless region and considerable anisotropy.

Received 28th March 2015
Accepted 1st May 2015

DOI: 10.1039/c5ra05502d

www.rsc.org/advances

1. Introduction

The binary molybdates with formula $RbLn(MoO_4)_2$, where Ln is a rare-earth element, are of great interest due to their diverse crystal structures and various catalytic, ion exchange and conductivity properties, luminescence, spectroscopic properties, optical properties and useful electro-physical properties.[1–11] The $RbLn(MoO_4)_2$ crystals are characterized by an acentric structure and possess pronounced piezoelectric and nonlinear optical properties, due to strong distortion of MoO_6 octahedrons.[12–20] Molybdates, with rare-earth ions, are promising candidates for manufacturing novel tunable optical materials and self frequency doubling laser medium .[21,22] Among these are the rare-earth containing crystals, particularly β-$RbSm(MoO_4)_2$. Atuchin *et al.*[23,24] have synthesized β-$RbSm(MoO_4)_2$ and investigated its structural properties and chemical bonding. The crystal structure of β-$RbSm(MoO_4)_2$ consists of layers of MoO_4 tetrahedrons, corner-sharing with SmO_8 square antiprisms. β-$RbSm(MoO_4)_2$ was found in the quasi-binary system $Rb_2MoO_4Sm_2(MoO_4)_3$, with a Rb : Sm ratio of 1 : 1, below the temperature 890–910 °C.[24] Recently Atuchin *et al.*[25] have prepared a β-$RbNd(MoO_4)_2$ microplate using the multistage solid state synthesis method. They studied the electronic structure using X-ray photoelectron spectroscopy (XPS) and X-ray emission spectroscopy (XES). They have also synthesized β-$RbNd(MoO_4)_2$ using a solid state reaction at T = 350–600 °C.[26,27] The crystal structure has been refined using the Rietveld method in the *Pbcn* space group. Due to their interesting structural, physical and chemical properties, the molybdate crystals have become potential candidates for enormous applications in photochemistry, optical technologies,[28–35] laser applications and electronics.[36–41]

It is clear that there is a lack of information regarding the electronic structure, optical properties and the electron charge density distribution of the microcrystalline β-$RbNd(MoO_4)_2$. Therefore, we thought it worthwhile to perform comprehensive density functional calculations based on the full potential method plus the Hubbard Hamiltonian (DFT+*U*) to investigate the electronic structure and the electron charge density distribution for the spin up (↑) and spin down (↓) states. Further insight into the electronic structure can be obtained from calculating and analyzing the spin up (↑) and spin down (↓) optical properties. It has been proven that the first-principles calculation is a strong and useful tool for predicting the crystal structure and its properties from the electron configuration of a material before its synthesis.[42–45]

2. Details of calculations

Microcrystalline rubidium neodymium dimolybdate, β-$RbNd(MoO_4)_2$, crystallizes in an orthorhombic structure with a *Pbcn* space group and cell parameters a = 5.1772(1) Å, b = 18.7293(4) Å, c = 8.2774(1) Å and v = 799.76(3) $Å^3$.[27] The crystal structure of the microcrystalline rubidium neodymium dimolybdate consists of complex layers perpendicular to the *b*-axis of the unit cell. The complex layers are formed by MoO_4 tetrahedrons sharing corners with NdO_8 square antiprisms as shown in

[a]*New Technologies – Research Centre, University of West Bohemia, Univerzitni 8, 306 14 Pilsen, Czech Republic. E-mail: maalidph@yahoo.co.uk; Fax: +420-386 361255; Tel: +420 777729583*

[b]*Center of Excellence Geopolymer and Green Technology, School of Material Engineering, University Malaysia Perlis, 01007 Kangar, Perlis, Malaysia*

Fig. 1(a)–(d). In Fig. 1(e) we illustrate the total energy as a function of the unit cell volume for both the paramagnetic and ferromagnetic states of β-RbNd$(MoO_4)_2$. It is clear that the paramagnetic state shows the lower energy indicating that the paramagnetic state is more stable. The experimental structural geometry[27] was optimized using the full potential linear augmented plane wave plus local orbitals (FPLAPW+lo) method[46] within the generalized gradient approximation (PBE−GGA).[47] For oxides and other highly correlated compounds, local density approximation (LDA) and GGA are known to fail to give the correct ground state. In these systems, the electrons are highly localized and the Coulomb repulsion between the electrons in open shells should be taken into account. Since there is no exchange correlation functional that can include this in an orbital independent way, a simpler approach is to add the Hubbard-like on-site repulsion to the Kohn–Sham Hamiltonian. This is known as a LDA+U or GGA+U calculation. There are different ways in which this can be implemented. In our work, we have used the method of Anisimov *et al.*[48] and Liechtenstein *et al.*[49] where the Coulomb (U) and exchange (J) parameters are used.

From the obtained relaxed geometry, the ground state properties were determined using FPLAPW+lo[50–53] within GGA+U (U-Hubbard Hamiltonian). We have applied U on the 4f orbital of Nd atoms and the 4d orbital of Mo atoms; the U values are 0.55 Ry and 0.22 Ry respectively. The potential for the construction of basis functions inside the sphere of the muffin tin was spherically symmetric, whereas outside the sphere it was constant. Self-consistency was obtained using 300 $\vec{k}$ points in the irreducible Brillouin zone (IBZ). The self-consistent calculations are converged since the total energy of the system is stable within 0.00001 Ry. The electronic band structure and the related properties were performed within 600 $\vec{k}$ points in the IBZ.

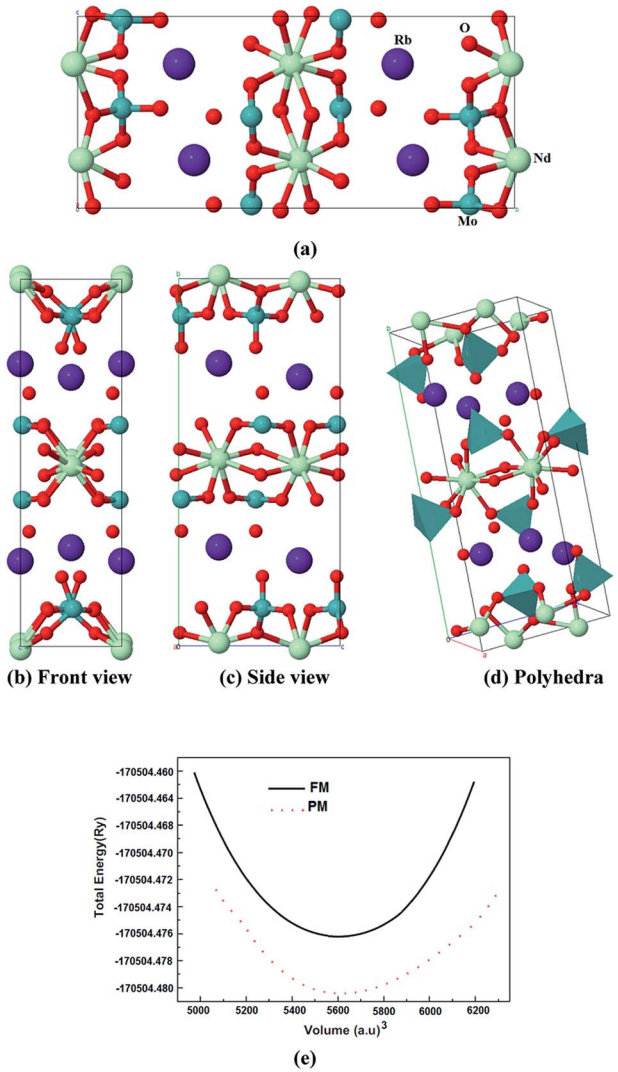

Fig. 1 (a) The crystal structure of β-RbNd$(MoO_4)_2$; (b) front view; (c) side view; (d) polyhedra. (e) The total energy as a function of unit cell volume for both the paramagnetic and ferromagnetic states of β-RbNd$(MoO_4)_2$. It is clear that the paramagnetic state shows the lower energy indicating that the paramagnetic state is more stable.

3. Results and discussion

The spin up (↑) and spin down (↓) electronic band structure of microcrystalline β-RbNd$(MoO_4)_2$ reveals that this compound is a direct band gap semiconductor as shown in Fig. 2(a) and (b). The valence band maximum (VBM) and the conduction band minimum (CBM) are located at the center of the first BZ for spin up (↑) and spin down (↓) cases. The calculated band gaps are 3.948 eV (↑) and 4.017 eV (↓). In these calculations, the zero of the energy scale is taken at the top of the valence band. It can be seen that the energy gap of the spin up (↑) case is lower than that of the spin down (↓) case. This is attributed to the location of Nd-f at around 5.0 eV for the spin up (↑) case which pushes the CBM towards the Fermi level, resulting in a reduction in the energy gap's value. For the spin down (↓) case, the Nd-f states are shifted towards higher energies by around 1.8 eV with respect to the position of Nd-f (↑), resulting in a shift of the CBM by around 0.069 eV towards higher energies and hence increasing the band gap's value of spin down (↓).

The necessary ingredients of the total and atom-resolved density of states are calculated for the spin up (↑) and spin down (↓) cases as shown in Fig. 3(b)–(f). The total density of states of the spin down (↓) case exhibits similar features to that of spin up (↑) except that the structure of Nd-f (around 5.0 eV (↑)) is merged with the other structures in the energy region between 5.5 and 7.5 eV (↓), and the CBM (↓) shifts towards higher energies by 0.069 eV. This observation supports the previous finding from the electronic band structure (Fig. 2(a) and (b)). The angular momentum character of the various structures in β-RbNd$(MoO_4)_2$ for the spin up (↑) and spin down (↓) states can be obtained from calculating the angular momentum projected density of states (PDOS). It has been found that the Rb-p state forms the structure around −7.5 eV for both spin up and spin down cases (Fig. 3(b)). The structure extended between −4.0 eV up to the Fermi level mainly originates from Mo-s/p/d, Nd-s/p/d, O1,2,3,4-p, Rb-s and Nd-f states for the spin up (↑) while for the spin down (↓) case, the same states are contributing except that the Nd-f state vanishes. The

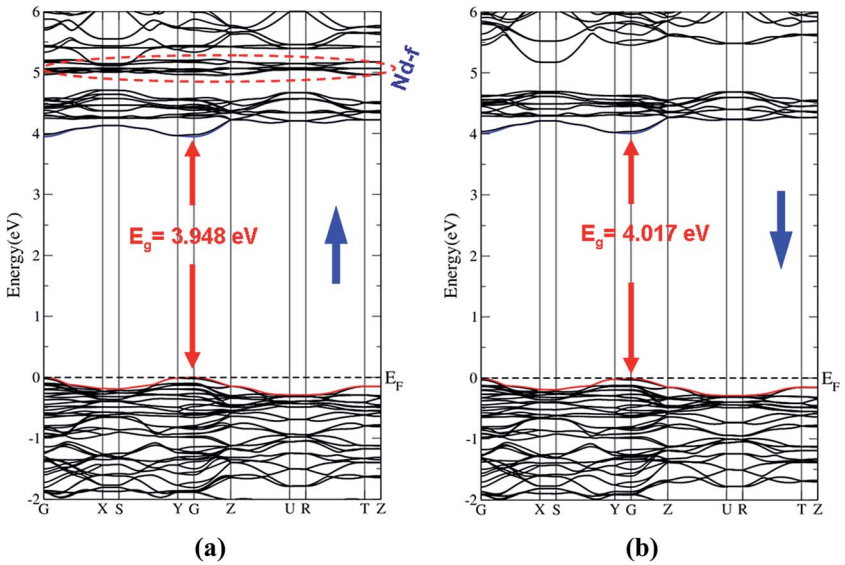

Fig. 2 Calculated electronic band structure of β-RbNd$(MoO_4)_2$: (a) spin up (↑); (b) spin down (↓).

structure from the CBM and above mainly originates from an admixture of Mo-s/p/d, Nd-s/p/d, and Rb-s/p states; these states contribute equally in the spin up (↑) and spin down (↓) cases. It has been found that O1,2,3,4-p states form the upper VB and exhibit a significant contribution in the VB, whereas the Mo-d state shows a significant contribution to the lower VB (this observation is in concordance with previous findings[25]).

The spin magnetic moments are calculated for the atom resolved within the muffin-tin spheres as well as in the interstitial sites as shown in Table 1. The calculated spin magnetic moments are in accordance with the Slater–Pauling rule. Calculations show that the magnetic moment of 4f electrons within the Nd sphere is about 2.988 μB. There exists a strong hybridization between Nd-d, Rb-d and Mo-d; Mo-p is hybridized with Nd-p and Rb-s; and the Nd-s state is hybridized with Rb-s and Nd-p states. The s-states of the four O atoms exhibit strong hybridization among each other and the same is observed for the p-states of the four O atoms. It is well-known that the strong hybridization may cause strong covalent bonding character. This can be investigated by calculating the valence band's electronic charge density distribution which helps in deeply visualizing the chemical bonding character and charge transfer. The calculated spin polarized total valence charge density distribution in (1 0 0) and (1 0 1) crystallographic planes for spin up (↑) and spin down (↓) are shown in Fig. 4(a)–(d). The electronegativity of Rb, Nd, Mo and O atoms according to the Pauling scale are 0.82, 1.14, 2.16 and 3.44, respectively.

The (1 0 0) crystallographic planes for spin up (↑) and spin down (↓) cases show that Mo atoms form strong covalent bonds with O atoms dependent on the Pauling electronegativity difference between these atoms, while Nd atoms form partially covalent and mostly ionic bonds with O atoms and Rb atoms exhibit ionic bond characters. For more details we have analyzed the spin polarized total valence charge density distribution in the (1 0 1) crystallographic plane for spin up (↑) and spin down (↓) cases. This plane confirms the existence of the partially covalent and mostly ionic bond between Nd–O, the strong covalent bond between Mo–O and the ionic bond character of Rb atoms. In all cases, the O atoms are surrounded by uniform blue spheres (indicating the maximum charge accumulation) which indicates that some valence electrons are transferred towards O atoms. The calculated bond distances in comparison to the measured ones[27] are listed in Table 2. Good agreement is found between the calculated and measured bond distances indicating the accuracy of the method of calculation.

For further insight into the spin polarized electronic structure, the spin polarized optical properties were calculated for majority spin (↑) and minority spin (↓) to ascertain the influence of the spin polarization on the optical properties.

The dielectric function $\varepsilon(\omega) = \varepsilon_1(\omega) + i\varepsilon_2(\omega)$ fully describes the optical properties of any homogeneous medium at all photon energies. In order to calculate the related dielectric tensor, the improved tetrahedron scheme[54] was applied for the BZ integration as provided in the WIEN2k package. Since the microcrystalline rubidium neodymium dimolybdate crystallizes in an orthorhombic structure, we need three dielectric tensor components to completely characterize the linear optical properties. The calculations of these dielectric functions involve the energy eigenvalues and electron wave functions. These are natural outputs of band structure calculations. We have performed calculations of the imaginary part of the inter-band frequency dependent dielectric function.[55]

The dielectric tensor components ${\varepsilon_2}^{xx}(\omega)$, ${\varepsilon_2}^{yy}(\omega)$ and ${\varepsilon_2}^{zz}(\omega)$ as shown in Fig. 5(a) exhibit a similar spectral structure for spin up (↑) and spin down (↓) cases except for minor differences in the peak heights and positions that are attributed to the differences in the absorption edges, which are 3.948 eV for spin up and 4.017 eV for spin down. Also the Nd-f states below the Fermi level (E_F) contribute in the spin up case only while

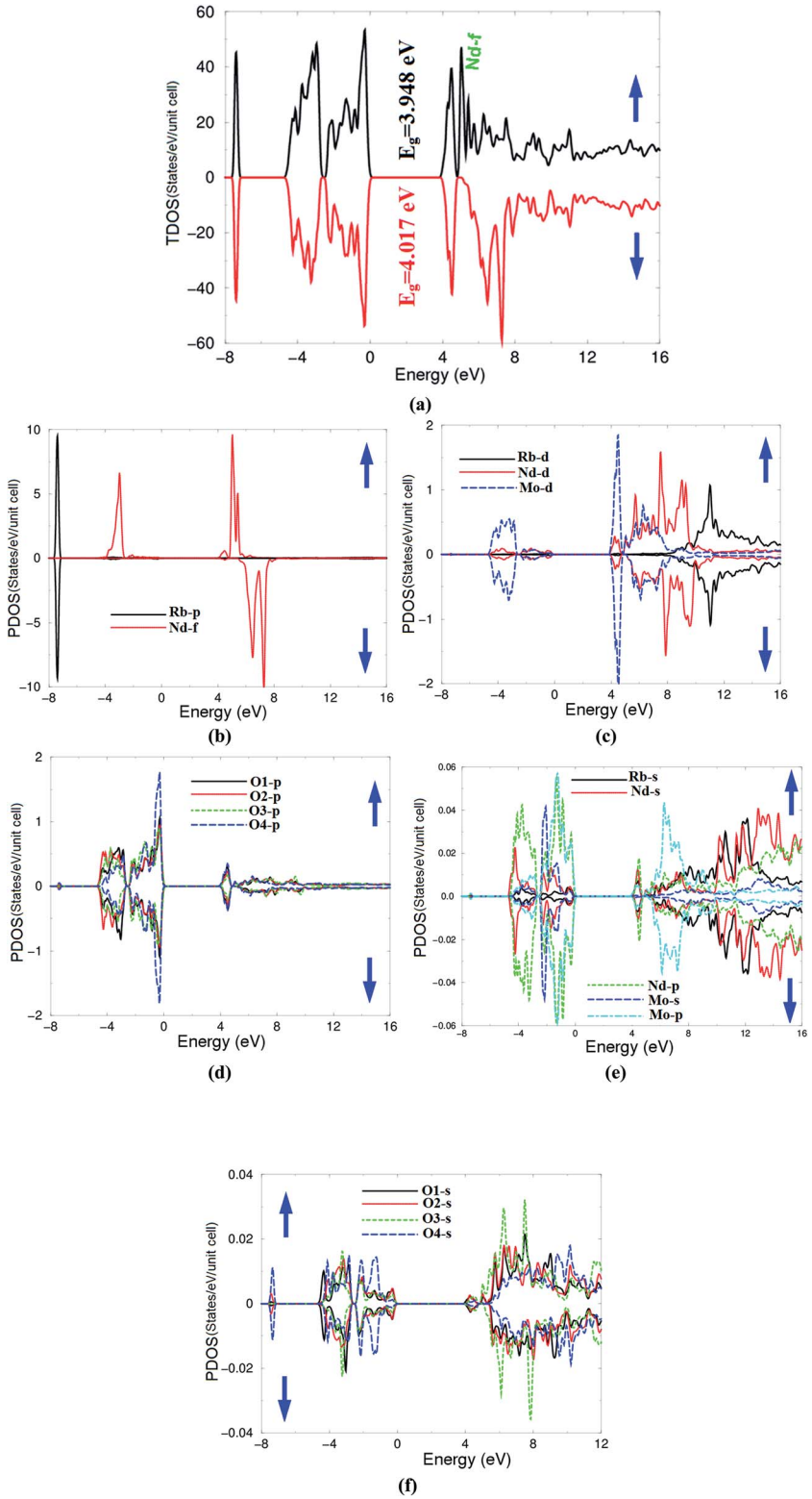

Fig. 3 Calculated total and partial density of states for spin up (↑) and spin down (↓).

they show zero contribution in the spin down case. The location and the contribution of Nd-f states above E_F have a significant influence for both spin up (↑) and spin down (↓) cases on the desperation of $\varepsilon_2{}^{xx}(\omega)$, $\varepsilon_2{}^{yy}(\omega)$ and $\varepsilon_2{}^{zz}(\omega)$. There exists a lossless region around 12.5 eV for both spin up and spin down cases. The three dielectric tensor components exhibit a considerable anisotropy in the energy region confined between 4.0 and 12.5 eV. The broadening is taken to be 0.1 eV

Table 1 Calculated atom-resolved spin magnetic moment (in μB)

Mo (μB)	Nd (μB)	Rb (μB)	O1 (μB)	O2 (μB)	O3 (μB)	O4 (μB)	Interst.(μB)
−0.00011	2.98826	−0.00003	−0.00474	−0.00339	−0.00680	−0.00077	0.17371

which is traditional for oxide crystals and is typical of the experimental accuracy needed to bring out all the structures.[56] The real part of the dielectric tensor components $\varepsilon_1^{xx}(\omega)$, $\varepsilon_1^{yy}(\omega)$ and $\varepsilon_1^{zz}(\omega)$ were calculated with the aid of the Kramers–Kronig transformation[57] and the existence information about $\varepsilon_2^{xx}(\omega)$, $\varepsilon_2^{yy}(\omega)$ and $\varepsilon_2^{zz}(\omega)$. These are illustrated in Fig. 5(b). The real

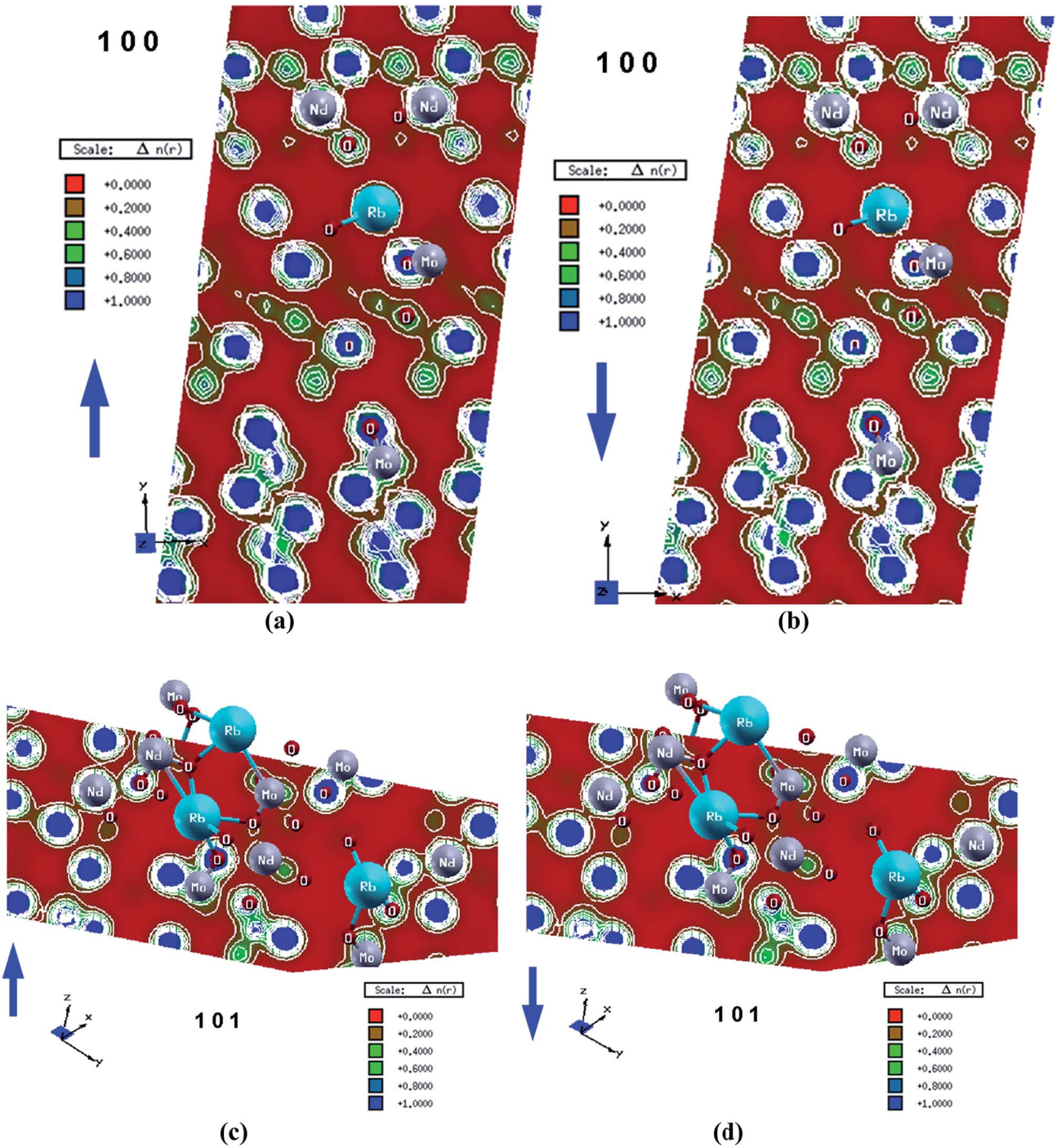

Fig. 4 Calculated electronic charge density distribution: (a) crystallographic plan (1 0 0) for spin up (↑) case; (b) crystallographic plan (1 0 0) for spin down (↓) case; (c) crystallographic plan (1 0 1) for spin up (↑) case; (d) crystallographic plan (1 0 1) for spin down (↓) case.

Table 2 The calculated inter-atomic distances in comparison with the measured ones[27]

	Bond lengths (Å)	
Bond	Exp.	Calc.
Rb–O4	2.71(2)	2.70
Rb–O4	2.96(2)	2.99
Rb–O2	2.95(2)	2.94
Nd–O3	2.44(4)	2.45
Nd–O1	2.42(2)	2.43
Nd–O2	2.48(2)	2.47
Nd–O3	2.74(4)	2.74
Mo–O1	1.74(2)	1.75
Mo–O2	1.72(2)	1.73
Mo–O3	1.85(2)	1.84
Mo–O4	1.74(2)	1.74

parts confirm the existence of the considerable anisotropy and the lossless region. We have calculated $\varepsilon_1{}^{xx}(0)$, $\varepsilon_1{}^{yy}(0)$ and $\varepsilon_1{}^{zz}(0)$ for spin up (↑) and spin down (↓). We should emphasize that $\varepsilon_1(0)$ corresponds to the optical dielectric constant, also know as ε_∞. This corresponds only to the electron contribution to the total dielectric constant. The values are listed in Table 3. We note that the spin up (↑) case exhibits larger $\varepsilon_1(0)$ values in comparison to the spin down (↓) case, which is attributed to the fact that the energy gap is about 3.948 eV for (↑) whereas it is 4.017 eV for (↓). Therefore, a smaller energy gap yields a larger $\varepsilon_1(0)$ value. This could be explained on the basis of the Penn model.[58] Penn proposed a relation between $\varepsilon(0)$ and E_g, $\varepsilon(0) \approx 1 + (\hbar\omega_p/E_g)^2$. E_g is some kind of averaged energy gap which could be related to the real energy gap. It is clear that $\varepsilon(0)$ is inversely proportional to E_g. In addition, we have calculated the uniaxial anisotropy $\delta\varepsilon = [(\varepsilon_0^{\parallel} - \varepsilon_0^{\perp})/\varepsilon_0^{tot}]$ for spin up (↑) and spin down (↓) cases as listed in Table 3. These values indicate the considerable anisotropy; the crystal exhibits negative uniaxial anisotropy.

Fig. 5(c) exhibits the loss function for spin up (↑) and spin down (↓). It is clear that the lossless region is almost zero along the energy range up to 9.0 eV. Above 9.0 eV, the lossless region significantly increases with increasing photon energy. The lossless region (9.0–12.5 eV) represents the plasma frequencies (ω_p). The absorption coefficients for the spin up (↑) and spin down (↓) cases were calculated and are presented in Fig. 5(d). It is clear that the absorption edge of the majority spin case is lower than that of the minority spin case. There exist three absorption regions: two of them exhibit low absorption, the first one extends from the fundamental energy band gap up to 6.0 eV and the second one from 11.0 eV and above, while the region (6.0 up to 11.0 eV) confined between those two regions, represents the high absorption region. In those three regions, the crystal exhibits high transparency for spin up and spin down. The calculated refractive indices for majority/minority spin are presented in Fig. 5(e). We have also calculated the refractive index at zero frequency $n^{xx}(0)$, $n^{yy}(0)$ and $n^{zz}(0)$ as presented in Table 3. We found that these values are higher for majority spin than for minority spin. This suggests that the refractive index at zero frequency is inversely related to the band gap. It confirms our previous finding that the spin up case possesses a lower band gap than the spin down.

The reflectivity spectra of β-RbNd$(MoO_4)_2$ for spin up and spin down exhibit a low reflectivity of about 5.0% at low energies up to 5.0 eV. This increases to be almost 20% on average along the whole energy range as illustrated in Fig. 5(f). The reflectivity minima occurs around 12.5 eV confirming the occurrence of collective plasmon resonance which represents the lossless regions in concordance with our observations in Fig. 5(a)–(d). In addition, we have calculated the imaginary and real parts of the optical conductivity, $\sigma(\omega)$ of β-RbNd$(MoO_4)_2$, for spin up and spin down cases as shown in Fig. 5(g) and (h). The optical conductivity of the materials is related to the complex dielectric function $\varepsilon(\omega) = \varepsilon_1(\omega) + i\varepsilon_2(\omega) = 1 + \frac{4\pi i\sigma(\omega)}{\omega}$. The imaginary part, $\sigma_2{}^{xx}(\omega)$, $\sigma_2{}^{yy}(\omega)$ and $\sigma_2{}^{zz}(\omega)$ as shown in Fig. 5(g), exhibit that the investigated material possesses zero optical conductivity at zero frequencies but it significantly increases with increasing photon energy to reach maximum values at 4.0 eV and 7.5 eV. The real part $\sigma_1{}^{xx}(\omega)$, $\sigma_1{}^{yy}(\omega)$ and $\sigma_1{}^{zz}(\omega)$ exhibit zero optical conductivity up to 3.5 eV, and thereafter the three components increase to reach maximum values at around 8.0 eV as shown in Fig. 5(h). The imaginary and real parts of the optical conductivity confirm the existence of the considerable anisotropy and the lossless region.

4. Conclusions

The spin polarized electronic band structure, total and partial density of states, chemical bonding and optical properties for the spin up (↑) and spin down (↓) cases of microcrystalline β-RbNd$(MoO_4)_2$ were calculated using the FPLAPW+lo method within GGA+*U*. The Hubbard Hamiltonian was applied on the 4f orbital of Nd atoms and 4d orbital of Mo atoms. The spin up (↑) and spin down (↓) electronic band structure indicate that β-RbNd$(MoO_4)_2$ is a direct band gap semiconductor with a spin up (↑) energy gap that is lower than that of the spin down (↓). This is attributed to the location of Nd-f at around 5.0 eV in the spin up (↑) case which pushes the CBM towards the Fermi level resulting in a reduction in the energy gap's value. For the spin down (↓) case, the Nd-f states are shifted towards higher energies by around 1.8 eV with respect to the spin up (↑) Nd-f position, resulting in a shift of the CBM by around 0.069 eV towards higher energies. This leads to an increase in the band gap of the spin down (↓) case. The calculated energy gap values are 3.948 eV (↑) and 4.017 eV (↓). To investigate the characters of the bonds, the total valence charge density distribution in the (1 0 0) and (1 0 1) crystallographic planes for spin up (↑) and spin down (↓) were calculated. The bond distances were calculated and compared to the measured ones and good agreement was found. To obtain deep insight into the electronic structure, the spin up (↑) and spin down (↓) optical properties were investigated. The calculated optical properties show that the β-RbNd$(MoO_4)_2$ crystal possesses negative uniaxial anisotropy and that there exists a lossless region and considerable anisotropy.

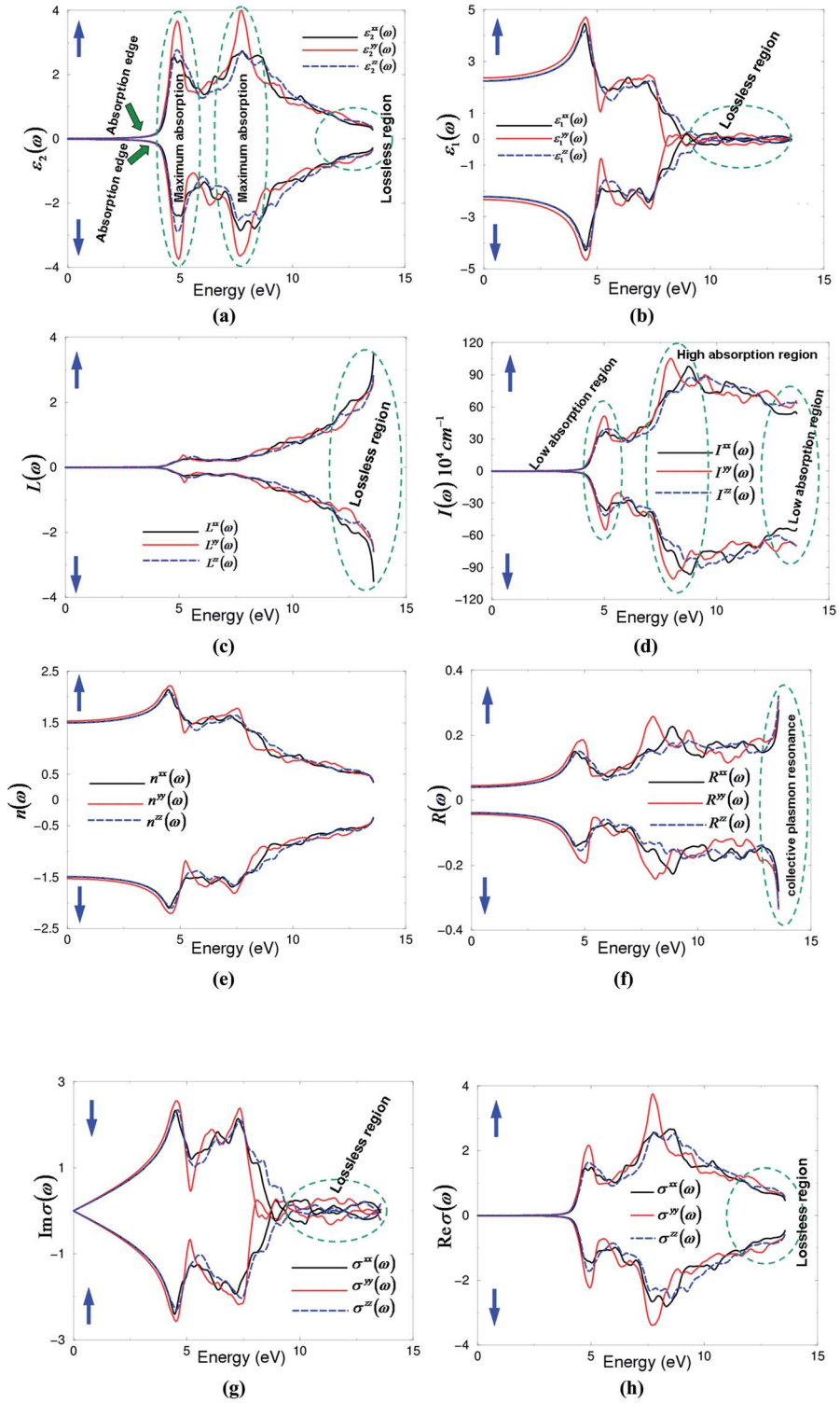

Fig. 5 (a) Calculated $\varepsilon_2{}^{xx}(\omega)$ (dark solid curve-black), $\varepsilon_2{}^{yy}(\omega)$ (light dashed curve-red) and $\varepsilon_2{}^{zz}(\omega)$ (light solid curve-blue) spectra for spin up (↑) and spin down (↓). (b) Calculated $\varepsilon_1{}^{xx}(\omega)$ (dark solid curve-black), $\varepsilon_1{}^{yy}(\omega)$ (light dashed curve-red) and $\varepsilon_1{}^{zz}(\omega)$ (light solid curve-blue) spectra for spin up (↑) and spin down (↓). (c) Calculated $L^{xx}(\omega)$ (dark solid curve-black), $L^{yy}(\omega)$ (light dashed curve-red) and $L^{zz}(\omega)$ (light solid curve-blue) spectra for spin up (↑) and spin down (↓). (d) Calculated absorption coefficient $I^{xx}(\omega)$ (dark solid curve-back), $I^{yy}(\omega)$ (light dashed curve-red) and $I^{zz}(\omega)$ (light solid curve-blue) spectra for spin up (↑) and spin down (↓). The absorption coefficient is given in 10^4 cm^{-1}. (e) Calculated $n^{xx}(\omega)$ (dark solid curve-black), $n^{yy}(\omega)$ (light dashed curve-red) and $n^{zz}(\omega)$ (light solid curve-blue) spectra for spin up (↑) and spin down (↓). (f) Calculated $R^{xx}(\omega)$ (dark solid curve-black), $R^{yy}(\omega)$ (light dashed curve-red) and $R^{zz}(\omega)$ (light solid curve-blue) spectra for spin up (↑) and spin down (↓). (g) Calculated $\sigma_2{}^{xx}(\omega)$ (dark solid curve-black), $\sigma_2{}^{yy}(\omega)$ (light dashed curve-red) and $\sigma_2{}^{zz}(\omega)$ (light solid curve-blue) spectra for spin up (↑) and spin down (↓). (h) Calculated $\sigma_1{}^{xx}(\omega)$ (dark solid curve-black), $\sigma_1{}^{yy}(\omega)$ (light dashed curve-red) and $\sigma_1{}^{zz}(\omega)$ (light solid curve-blue) spectra for spin up (↑) and spin down (↓).

Table 3 Calculated $\varepsilon_1^{xx}(\omega)$, $\varepsilon_1^{yy}(\omega)$, $\varepsilon_1^{zz}(\omega)$, $\varepsilon_1^{tot}(\omega)$ and $\delta\varepsilon$ at static limit and $\lambda = 450$ nm

	At static limit		At $\lambda = 450$ nm	
Components	Spin up	Spin dn	Spin up	Spin dn
$\varepsilon_1^{xx}(\omega)$	2.260	2.218	2.571	2.505
$\varepsilon_1^{yy}(\omega)$	2.366	2.330	2.720	2.665
$\varepsilon_1^{zz}(\omega)$	2.260	2.220	2.571	2.515
$\varepsilon_1^{tot}(\omega)$	2.295	2.254	2.620	2.561
$\delta\varepsilon$	−0.0461	−0.0492	−0.0568	−0.0605

Acknowledgements

The results were developed within the CENTEM project, reg. no. CZ.1.05/2.1.00/03.0088, cofunded by the ERDF as part of the Ministry of Education, Youth and Sports OP RDI programme and, in the follow-up sustainability stage, supported through CENTEM PLUS (LO1402) by financial means from the Ministry of Education, Youth and Sports under the "National Sustainability Programme I". Computational resources were provided by MetaCentrum (LM2010005) and CERIT-SC (CZ.1.05/3.2.00/08.0144) infrastructures.

References

1 O. D. Chimitova, B. G. Bazarov, K. N. Fedorov and L. G. Bazarova, *Buryat State University Bulletin, Ser. 1: Chemistry*, 2005, no. 2, pp. 37–40.
2 B. G. Bazarov, R. F. Klevtsova, O. D. Chimitova, K. N. Fedorov, L. A. Glinskaya, Y. L. Tushinova and L. G. Bazarova, *Russ. J. Inorg. Chem.*, 2006, **51**(5), 794–799.
3 O. D. Chimitova, B. G. Bazarov, R. F. Klevtsova, K. N. Fedorov, L. A. Glinskaya, M. V. Kuznetsov and L. G. Bazarova, *Russ. Chem. Bull.*, 2007, **56**(11), 2135–2139.
4 C. V. Ramana, V. V. Atuchin, V. G. Kesler, V. A. Kochubey, L. D. Pokrovsky, V. Shutthanandan, U. Becker and R. C. Ewing, *Appl. Surf. Sci.*, 2007, **253**(12), 5368–5374.
5 C. V. Ramana, V. V. Atuchin, L. D. Pokrovsky, U. Becker and C. M. Julien, *J. Vac. Sci. Technol., A*, 2007, **25**(4), 1166–1171.
6 B. G. Bazarov, O. D. Chimitova, R. F. Klevtsova, Y. L. Tushinova, L. A. Glinskaya and L. G. Bazarova, *J. Struct. Chem.*, 2008, **49**(1), 53–57.
7 O. D. Chimitova, B. G. Bazarov, K. N. Fedorov and L. G. Bazarova, *J. Appl. Chem.*, 2008, **11**, 1928–1929.
8 V. V. Atuchin, T. A. Gavrilova, V. G. Kostrovsky, L. D. Pokrovsky and I. B. Troitskaia, *Inorg. Mater.*, 2008, **44**(6), 622–627.
9 B. G. Bazarov, O. D. Chimitova, C. T. Bazarova, S. I. Arkhincheeva and L. G. Bazarova, *Russ. J. Inorg. Chem.*, 2008, **53**(6), 959–961.
10 C. V. Ramana, V. V. Atuchin, I. B. Troitskaia, S. A. Gromilov, V. G. Kostrovsky and G. B. Saupe, *Solid State Commun.*, 2009, **149**, 6–9.
11 C. V. Ramana, I. B. Troitskaia, V. V. Atuchin, M. Ramos and D. Ferrer, *J. Vac. Sci. Technol., A*, 2010, **28**(4), DOI: 10.1116/1.3397791.
12 P. S. Halasyamani and K. P. Poeppelmeier, *Chem. Mater.*, 1998, **10**, 2753–2769.
13 B. I. Kidyarov and V. V. Atuchin, *Ferroelectrics*, 2007, **360**, 96–99.
14 B. I. Kidyarov and V. V. Atuchin, *Ferroelectrics*, 2007, **360**, 104–110.
15 V. V. Atuchin and B. I. Kidyarov, *Journal of the Korean Crystal Growth and Crystal Technology*, 2002, **12**(6), 323–328.
16 E. Sykora Richard, M. Ok Kang, P. S. Halasyamani and E. AlbrechtSchmitt Thomas, *J. Am. Chem. Soc.*, 2002, **124**(9), 1951–1957.
17 V. V. Atuchin, B. I. Kidyarov and N. V. Pervukhina, *Comput. Mater. Sci.*, 2004, **30**(3–4), 411–418.
18 V. Krivovichev Sergey, J. Locock Andrew and C. Bums Peter, *Z. Kristallogr.*, 2005, **220**, 10–18.
19 A. Solodovnikova Zoya and F. Solodovnikov Sergey, *Acta Crystallogr., Sect. C: Cryst. Struct. Commun.*, 2006, **62**, i53–i56.
20 O. Chi Eun, M. Ok Kang, Y. Porter and P. S. Halasyamani, *Chem. Mater.*, 2006, **18**, 2070–2074.
21 O. D. Chimitova, V. V. Atuchin, B. G. Bazarov, M. S. Molokeev and Z. G. Bazarova, *Proc. SPIE*, 2013, 87711A.
22 V. V. Atuchin, O. D. Chimitova, S. V. Adichtchev, B. G. Bazarov, T. A. Gavrilova, M. S. Molokeev, N. V. Surovtsev and Z. G. Bazarova, *Mater. Lett.*, 2013, **106**, 26–29.
23 V. V. Atuchin, O. D. Chimitova, S. V. Adichtchev, J. G. Bazarov, T. A. Gavrilova, M. S. Molokeev, N. V. Surovtsev and Z. G. Bazarova, *Mater. Lett.*, 2013, **106**, 26–29.
24 V. V. Atuchin, A. S. Aleksandrovsky, O. D. Chimitova, C.-P. Diao, T. A. Gavrilova, V. G. Kesler, M. S. Molokeev, A. S. Krylov, B. G. Bazarov, J. G. Bazarova and Z. Lin, *Dalton Trans.*, 2015, 1805.
25 V. V. Atuchin, O. Y. Khyzhun, O. D. Chimitova, M. S. Molokeev, T. A. Gavrilova, B. G. Bazarov and J. G. Bazarova, *J. Phys. Chem. Solids*, 2015, **77**, 101–108.
26 V. V. Atuchin, O. D. Chimitova, T. A. Gavrilova, B. G. Bazarov and J. G. Bazarova, XI International Conference and Seminar EDM'2010, Section I, June 30 – July 4, ERLAGOL.
27 V. V. Atuchin, O. D. Chimitova, T. A. Gavrilova, M. S. Molokeev, S.-J. Kim, N. V. Surovtsev and B. G. Bazarov, *J. Cryst. Growth*, 2011, **318**, 683–686.
28 T. T. Basiev, A. A. Sobol, Y. Voronko and P. G. Zverev, *Opt. Mater.*, 2000, **15**, 205–216.
29 Z. L. Gao, X. T. Tao, X. Yin, W. G. Zhang and M. H. Jiang, *Appl. Phys. Lett.*, 2008, **93**, 252906.
30 G. P. Cai, J. Y. Wang and H. J. Zhang, *Cryst. Res. Technol.*, 2009, **44**, 1001–1004.
31 M. Mączka, A. Pietraszko, W. Paraguassu, A. G. Souza Filho, P. T. C. Freire, J. Mendes Filho, P. T. C. Freire, J. Mendes Filho and J. Hanuza, *J. Phys.: Condens. Matter*, 2009, **21**, 095402.
32 T. Namsaraeva, B. Bazarov, D. Mikhailova, N. Kuratieva, A. Sarapulova, A. Senyshyn, *et al.*, *Eur. J. Inorg. Chem.*, 2011, 2832–2841.
33 J. J. Zhang, Z. L. Gao, X. Yin, Z. H. Zhang, Y. X. Sun and X. T. Tao, *Appl. Phys. Lett.*, 2012, **101**, 062901.

34 V. V. Atuchin, V. G. Grossman, S. V. Adichtchev, N. V. Surovtsev, T. A. Gavrilova and B. G. Bazarov, *Opt. Mater.*, 2012, **34**, 812–816.

35 C. S. Lim, *Mater. Res. Bull.*, 2012, **47**, 4220–4225.

36 P. V. Klevtsov and R. F. Klevtsova, *J. Struct. Chem.*, 1977, **18**(3), 419.

37 T. T. Basiev, A. A. Sobol, Y. K. Voronko and P. G. Zverev, *Opt. Mater.*, 2000, **15**, 205.

38 F. E. Osterloh, *Chem. Mater.*, 2008, **20**, 35.

39 A. Kudo and Y. Miseki, *Chem. Soc. Rev.*, 2009, **38**, 253.

40 M. Maczka, A. G. Souza Filho, W. Paraguassu, P. T. C. Freire, J. Mendes Filho and J. Hanuza, *Prog. Mater. Sci.*, 2012, **57**, 1335.

41 O. D. Chimitova, V. V. Atuchin, B. G. Bazarov, M. S. Molokeev and Z. G. Bazarova, *Proc. SPIE*, 2013, **8771**, 87711A.

42 A. H. Reshak and S. Auluck, *RSC Adv.*, 2014, **4**, 37411.

43 A. H. Reshak, *RSC Adv.*, 2014, **4**, 39565.

44 M. Jamal, N. Kamali Sarvestani, A. Yazdani and A. H. Reshak, *RSC Adv.*, 2014, **4**, 57903.

45 A. H. Reshak, *RSC Adv.*, 2014, **4**, 63137; A. H. Reshak, *RSC Adv.*, 2015, **5**, 33632.

46 P. Blaha, K. Schwarz, G. K. H. Madsen, D. Kvasnicka and J. Luitz, *WIEN2k, An augmented plane wave plus local orbitals program for calculating crystal properties*, Vienna University of Technology, Austria, 2001.

47 J. P. Perdew, S. Burke and M. Ernzerhof, *Phys. Rev. Lett.*, 1996, **77**, 3865.

48 V. I. Anisimov, I. V. Solvyev, M. A. Korotin, M. T. Czyzyk and C. A. Sawatzky, *Phys. Rev. B: Condens. Matter Mater. Phys.*, 1993, **48**, 16929.

49 A. I. Liechtenstein, V. I. Anisimov and J. Zaanen, *Phys. Rev. B: Condens. Matter Mater. Phys.*, 1995, **52**, R5467.

50 O. K. Andersen, *Phys. Rev.*, 1975, **B12**, 3060.

51 J. P. Perdew and Y. Wang, *Phys. Rev. B: Condens. Matter Mater. Phys.*, 1992, **45**, 13244.

52 J. P. Perdew, K. Burke and M. Ernzerhof, *Phys. Rev. Lett.*, 1996, **77**, 3865.

53 K. Schwarz and P. Blaha, *Comput. Mater. Sci.*, 2003, **28**, 259.

54 O. Jepsen and O. K. Andersen, *Solid State Commun.*, 1971, **9**, 1763; G. Lehmann and M. Taut, *Phys. Status Solidi B*, 1972, **54**, 496.

55 S. Hufner, R. Claessen, F. Reinert, T. Straub, V. N. Strocov and P. Steiner, *J. Electron Spectrosc. Relat. Phenom.*, 1999, **100**, 191.

56 A. Hussain Reshak, X. Chen, S. Auluck and I. V. Kityk, *J. Chem. Phys.*, 2008, **129**, 204111.

57 F. Wooten, *Optical Properties of solids*, Academic press, New York and London, (1972).

58 D. R. Penn, *Phys. Rev. B: Condens. Matter Mater. Phys.*, 1962, **128**, 2093.